Monthly Notices
of the
ROYAL ASTRONOMICAL SOCIETY

MNRAS **481,** 3902–3920 (2018)
Advance Access publication 2018 August 30

doi:10.1093/mnras/sty2354

New Galactic star clusters discovered in the disc area of the VVVX survey

J. Borissova,[1,2★†] V. D. Ivanov,[3★] P. W. Lucas,[4★] R. Kurtev,[1,2] J. Alonso-Garcia,[2,5] S. Ramírez Alegría,[5] D. Minniti,[2,6] D. Froebrich,[7] M. Hempel,[2,8] N. Medina,[1,2] A.-N. Chené[9] and M. A. Kuhn[2,10]

[1]*Instituto de Física y Astronomía, Universidad de Valparaíso, Av. Gran Bretaña 1111, Playa Ancha, Casilla 5030, Chile*
[2]*Millennium Institute of Astrophysics (MAS), Santiago, Chile*
[3]*European Southern Observatory, Karl Schwarzschildstr. 2, D-85748 Garching bei München, Germany*
[4]*Centre for Astrophysics, University of Hertfordshire, College Lane, Hatffeld AL10 9AB, UK*
[5]*Centro de Astronomía (CITEVA), Universidad de Antofagasta, Avenida Angamos 601, Antofagasta, Chile*
[6]*Departamento de Física, Facultad de Ciencias Exactas, Universidad Andés Bello, Av. Fernandez Concha 700, Las Condes, Santiago, Chile*
[7]*Centre for Astrophysics and Planetary Science, School of Physical Sciences, University of Kent, Canterbury CT2 7NH, UK*
[8]*Instituto de Astrofísica, Pontificia Universidad Católica de Chile, Casilla 306, Santiago 22, Chile*
[9]*Gemini Observatory, Northern Operations Center, 670 A'ohoku Place, Hilo, HI 96720, USA*
[10]*Department of Astronomy, California Institute of Technology, Pasadena, CA 91125, USA*

Accepted 2018 August 28. Received 2018 August 28; in original form 2018 January 31

ABSTRACT

The 'VISTA Variables in the Vía Láctea eXtended (VVVX)' ESO Public Survey is a near-infrared photometric sky survey that covers nearly 1700 deg^2 towards the Galactic disc and bulge. It is well-suited to search for new open clusters, hidden behind dust and gas. The pipeline processed and calibrated K_S-band tile images of 40 per cent of the disc area covered by VVVX was visually inspected for stellar overdensities. Then, we identified cluster candidates by examination of the composite JHK_S colour images. The colour–magnitude diagrams of the cluster candidates are constructed. Whenever possible the *Gaia* DR2 parameters are used to calculate the mean proper motions, radial velocities, reddening and distances. We report the discovery of 120 new infrared clusters and stellar groups. Approximately half of them (47 per cent) are faint, compact, highly reddened, and they seem to be associated with other indicators of recent star formation, such as nearby Young Stellar Objects, Masers, H II regions or bubbles. The preliminary distance determinations allow us to trace the clusters up to 4.5 kpc, but most of the cluster candidates are centred at 2.2 kpc. The mean proper motions of the clusters show that in general they follow the disc motion of the Galaxy.

Key words: Galaxy: open clusters and associations: general – Galaxy: disk – Infrared: stars.

1 INTRODUCTION

The Milky Way environment provides a unique place to test the predictions of cosmological models and the theories of galaxy formation. Moreover, our location within our own Galaxy gives us a close-up look at star clusters which in turn has implications on extragalactic star clusters studies with the next generation facilities like the NASA's James Webb Space Telescope (JWST) and the ESO's European Extremely Large Telescope (E-ELT). In preparation for these we have to complete the census of star clusters in the Galaxy, as well as to create template samples of well-understood benchmark star clusters. This has motivated the renewed interest in star clusters, made possible by the new all-sky infrared (IR) surveys, such as 2MASS (Two Micron All Sky Survey; Skrutskie et al. 2006), GLIMPSE (Galactic Legacy Infrared Mid-Plane Survey Extraordinaire; Benjamin et al. 2003), WISE (Wide-field Infrared Survey Explorer; Wright et al. 2010), VVV (VISTA Variables in the Vía Láctea; Minniti et al. 2010) and UKIDSS GPS (The Galactic Plane Survey; Lucas et al. 2008). These new IR surveys added many new objects to the traditional optical catalogues [e.g. WEBDA Dias et al. (2002); MWSC or Milky Way global survey of Star Clusters data base – Kharchenko et al. 2013, Schmeja et al. 2014], including some heavily obscured star clusters visible only in the infrared (hereafter IR clusters; see for example Morales et al. 2013; Zasowski et al. 2013; Camargo, Bica & Bonatto 2016). Taking into account the re-

★ E-mail: jura.borissova@uv.cl (JB); vivanov@eso.org (VDI); p.w.lucas@herts.ac.uk (PWL)
† Based on observations gathered with VIRCAM at the ESO VISTA telescope, as part of observing programmes 198.B-2004.

sent work of Ryu & Lee (2018), the total number of known infrared clusters has now exceeded 6300 objects.

Many of these new IR clusters are based on the ESO Large Public Survey VISTA Variables in the Vía Láctea – VVV,[1] because it delivered deep sub-arcsec seeing $ZYJHK_S$ images and photometry (Minniti et al. 2010; Saito et al. 2012). The VVV survey mapped the IR variability of the Milky Way bulge and southern mid-plane over a period of six years (2010–2016). The VVV footprint contained about 300 known clusters, but more than 750 new clusters and candidate clusters were added in VVV-based works (e.g. Borissova et al. 2011, 2014; Solin, Haikala & Ukkonen 2014; Barbá el al. 2015; Ivanov et al. 2017; Froebrich et al. 2017). Follow-up spectroscopy of some new candidates confirmed their cluster nature, improving the census of young massive clusters in the Galaxy: seven new ones were added and they contain at least one newly discovered WR star (Chené et al. 2013, 2015; Hervé et al. 2016). We have reported a new, massive WR star (>100 solar mass, Chené et al. 2015), a new, massive cluster in the far edge of the Galactic bar (Ramírez Alegría et al. 2014), etc. The multi-epoch K_S VVV observations also made it possible to investigate the IR variability of the cluster members (Borissova et al. 2014, 2016; Navarro Molina et al. 2016; Medina et al. 2018).

The existence of these previously undiscovered open clusters was predicted by Portegies Zwart, McMillan & Gieles (2010), but the VVV survey has also improved the census of globular clusters in the Galactic bulge and disc. The number of globular clusters in our Galaxy was estimated to be not more than 160 (see Ivanov, Kurtev & Borissova 2005, for an empirical approach to the missing globular clusters). But recent discoveries in the VVV area reveal about 100 new globular cluster candidates (Minniti et al. 2011, 2017a,b; Moni Bidin et al. 2011; Borissova et al. 2014; Minniti, Alonso-García & Pullen 2017c). If confirmed, this will drastically change the landscape of the old cluster population in our Galaxy.

A new project, 'VISTA Variables in the Vía Láctea eXtended' (VVVX) survey, was launched in 2016 as an extension of the complied VVV survey in order to enhance its legacy value. The VVVX will spend a total of ∼2000 h of VISTA time over 3 years to extend the VVV time-baseline and to nearly double the VVV spatial coverage up to ∼1700 deg^2 from $l = 230^\circ$ to $l = 20^\circ$ (7^h, $< \alpha < 19^h$). Based on the VVV experience, our predictions are that VVVX will also significantly increase the number of star clusters in our Galaxy. Many are expected near the tangent point of the Carina arm region, which harbours very massive young clusters such as Westerlund 2, NGC 3603 and the Carina Nebula Complex. The extension of VVVX towards the third Galactic quadrant is fundamental to unveil new clusters along the Perseus arm and to trace the proposed Outer arm, reaching the edge of the Galactic disc.

Thus, following Borissova et al. (2011) we expanded our investigation of the Milky Way cluster population to include the new areas covered by VVVX, aiming to improve the star cluster census and to continue building a statistically significant sample of clusters, with homogeneously derived parameters. We concentrate on objects that are practically invisible in the optical bands. The improved catalogue of star clusters in the Galaxy can help to constrain theoretical models of cluster formation (e.g. Pfalzner et al. 2016) and to determine some fundamental relations between basic cluster parameters.

Two and a half years after the start of the VVVX survey we have at our disposal only a part of the VVVX footprint. In this paper, we report the first results of our visual search for new star cluster candidates in the VVVX disc area. More specifically by 2018 April, approxf. 55 per cent of the new VVVX area was observed. From this, we have searched 74 per cent, excluding only the extension of the VVVX bulge, which we plan to examine by automated tools. With respect to the whole new VVVX area the total area searched in this paper is 40 per cent.

2 OBSERVATIONS AND DATA REDUCTION

The VVV and VVVX data were obtained with the 4.1-m ESO VISTA telescope (Visual and Infrared Survey Telescope for Astronomy; Emerson, McPherson & Sutherland 2006) located at Cerro Paranal, Chile, with the 16-detector VIRCAM (VISTA Infrared CAMera; Dalton et al. 2006). It has an $\sim 1 \times 1.5$ deg^2 field of view and works in the 0.9–2.5 μm wavelength range and a pixel scale of 0.34 arcsec pixel^{-1}. The data are reduced with the VISTA Data Flow System (VDFS; Emerson et al. 2004; Irwin et al. 2004) at the Cambridge Astronomical Survey Unit[2] (CASU). Processed images and photometric catalogues are available from the ESO Science Archive[3] and from the VISTA Science Archive[4] (VSA; Cross et al. 2012). A single VIRCAM image, called paw, contains large gaps; six paws taken in a spatial offset pattern must be combined to fill them in, obtaining a contiguous image, called tile. The VVVX paws and tiles are aligned along l and b. The total exposure time of the tiles are: 8 s in K_S (for a single epoch), 24 s in H and 60 in J band. The tiles overlap by a few arcmin in Galactic latitude and longitude – just like with the VVV – to ensure homogeneous coverage, spatial continuity and overall photometric and astrometric consistency. The tile overlaps result in a small fraction of duplicate sources, which is advantageous for variable stars, but that must be taken into account when analysing maps or star counts that span wider areas than that of a single tile. Importantly, these tile overlaps allow to test the intrinsic accuracy of the photometry and astrometry. Therefore, the VVVX followed the same observing strategy as the VVV.

Fig. 1 shows the VVV and VVVX footprints. In the bulge this corresponds to $20^\circ \times 24^\circ$ (14×22 tiles). These are shown in Fig. 1 in red for the former VVV tiles (b201 to b396), in cyan for the new southern bulge extension from tiles b401 to b456, and for the new northern bulge extension from tiles b457 to b512. The new northern disc area covers a $10^\circ \times 9^\circ$ patch (7×8 tiles). These are shown in green in Fig. 1, from tiles e933 to e988. The new southern disc area covers $120^\circ \times 9^\circ$, split into two stripes of 83×2 tiles each (Fig. 1; tiles e601 to e766, and e767 to e932 are marked in blue) and an extension along the Galactic mid-plane region by $65^\circ \times 4^\circ$, (Fig. 1, tiles e1001 to e1180 are shown in yellow). The original VVV-disc area is also shown in red in Fig. 1, consisting of tiles d001 to d152. During its first two and a half years (2016 to 2018), the VVVX survey covered in the JHK_S bands the southern bulge extension from tiles b401 to b456, e601 to e766, and e767 to e932. The northern disc tiles are from e933 to e988.

3 CLUSTER SEARCH AND VALIDATION

Our previous experience has shown that the number densities used by automated cluster searches (Ivanov et al. 2002; Borissova et al. 2003) tend to yield a large number of spurious cluster candidates

[1] P.I. D. Minniti, https://vvvsurvey.org

[2] http://casu.ast.cam.ac.uk/

[3] http://archive.eso.org/

[4] http://horus.roe.ac.uk/vsa/

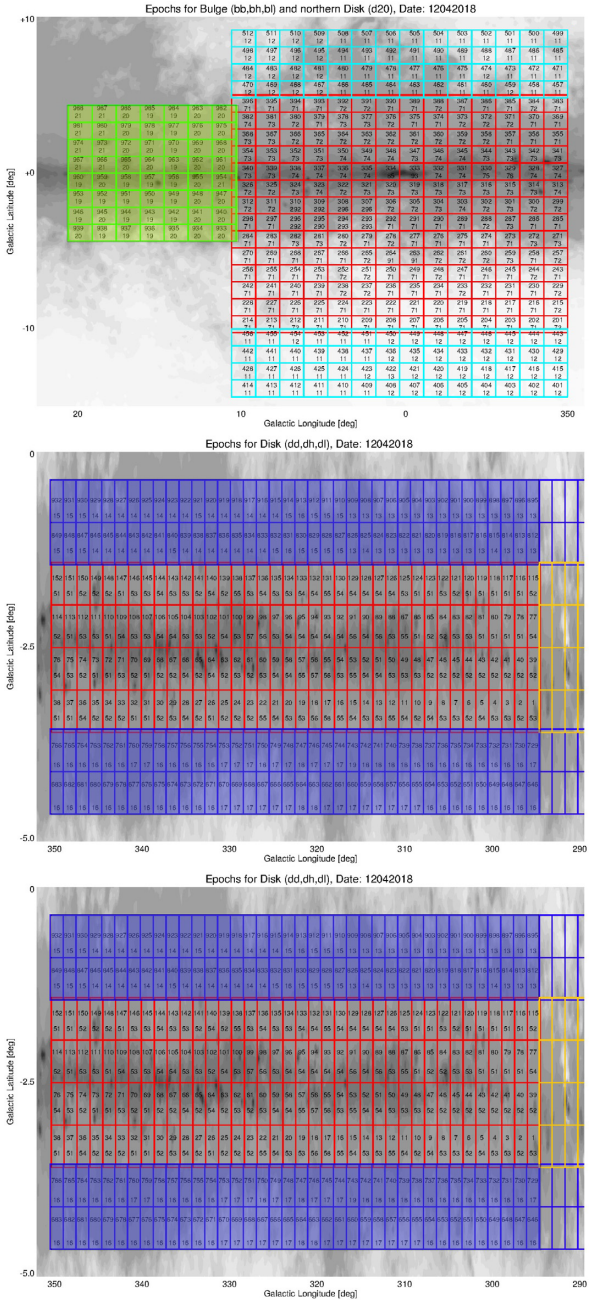

Figure 1. The VVVX Survey area. The red squares show the VVV Survey tiles, the green the Northern disc extension, the cyan the bulge area extension, the blue the extensions of both sides of the South VVV disc, and the yellow new VVVX outer disc fields. The searched areas are filled with green and dark blue colours. The numbers in each tile are its identification number (top) and the number of K_S epochs by 2018 April 12.

in the inner Milky Way, because of the uneven distribution of the obscuring dust. They require time-consuming manual follow up at different, e.g. mid-IR, wavelengths, and at the end they are not much more effective than simple visual searches. Furthermore, here we are aiming at relatively faint and heavily reddened clusters, undiscovered in the 2MASS, DENIS and GLIMPSE surveys. Therefore, we adopted the visual inspection as our search method. All observed images were retrieved from the CASU database and initially the K_S tile images were visually inspected. The preliminary list of candidates was created on the basis of the detected local overdensity of the number of stars with respect to the surrounding area. Then, the composite JHK_S colour images were created and we verified the compact appearance, distinctive from the surrounding field and containing at least five to six stars with similar colours concentrated towards the objects' centre. Fig. 2 shows the composite JHK_S colour images of some newly discovered cluster candidates and stellar groups for illustration. The colour images of the whole sample are given in Appendix C.

The next step in our validation process was the analysis of the colour–magnitude diagrams. To construct them, we performed PSF photometry of a 2.5 × 2.5 arcmin^2 area in the J, H, and K_S bands surrounding the selected candidate. We used the Dophot photometric routine following Alonso-García et al. (2017). The instrumental magnitudes were transformed to the standard system, and the saturated stars (usually $K_S \leq 11.5$ mag, depending on crowding) were replaced by 2 MASS stars (2MASS PSC; Skrutskie et al. 2006). This procedure is described in detail by Alonso-García et al. (2017) and Borissova et al. (2011, 2014). Fig. 3 shows two examples of colour–magnitude diagrams for VVVX CL076 and VVVX CL077, both classified as open clusters. The most probable cluster members are selected by statistical decontamination procedure (for more details see Borissova et al. 2011) and *Gaia* DR2 proper motion diagrams (see the next paragraph). Following Zasowski et al. (2013), we then fit the Padova theoretical isochrones with solar metallicity (Bressan et al. 2012) (http://stev.oapd.inaf.it/cgi-bin/cmd). The best fit for VVVX CL076 is 32 Myr, while VVVX CL077 is most probably 10 Myr old. We used the *Gaia* RD2 parallaxes as initial values for the distances (see Table B1), while the mean reddening is determined in the interactive process of the fitting as $E(J - K_S) = 1.6 \pm 0.2$ and $E(J - K_S) = 1.7 \pm 0.2$, respectively. The colour–magnitude diagrams of the whole sample, excluding very faint and compact candidates, are given in Appendix D. The ages of the cluster candidates, however, will be a subject of follow-up paper, together with up-coming spectroscopic data.

The *Gaia* astrometric mission was launched in 2013 December (Gaia Collaboration et al. 2016) to measure positions, parallaxes, proper motions and photometry for over 10^9 sources as well as to obtain physical parameters and radial velocities for millions of stars. Its recent Data Release 2 (*Gaia* DR2) has covered the initial 22 months of data taking (Gaia Collaboration et al. 2018). As pointed out by Gaia Collaboration et al. (2018b), it is expected that the members of the clusters span small range of distances and their members follow a common space motion which is, in general, different from the bulk of the field stars in the same region. This is illustrated in Fig. 4 (lower panel) for the massive open cluster Danks 2. Thus, we can select the stars with common proper motion and their mean parallax can give us the distance to the cluster. In our case, only a small number of probable cluster members have *Gaia* DR2 counterparts, because we are covering the infrared bands and fainter stars. Moreover, the cluster members are moving with the disc and it is hard to distinguish between both motions.

Therefore, we adopted the following procedure: the most probable cluster members from the statistically decontaminated K_S versus $(J - K_S)$ diagrams (Fig. 4, upper, red solid circles) are cross-matched with *Gaia* DR2 catalogue (middle, red solid circles). The proper motion vector diagrams μ_δ versus $\mu_\alpha \cos\delta$ are created and the stars with obviously different proper motion are rejected. Whenever possible, the histograms of radial velocities are also examined and the outliers are rejected. For such 'cleaned' sample of probable cluster members we calculated the median value and the standard deviation of $\mu_\alpha \cos\delta$ and μ_δ (Col: 4 to 7 of Table B1), which we consider

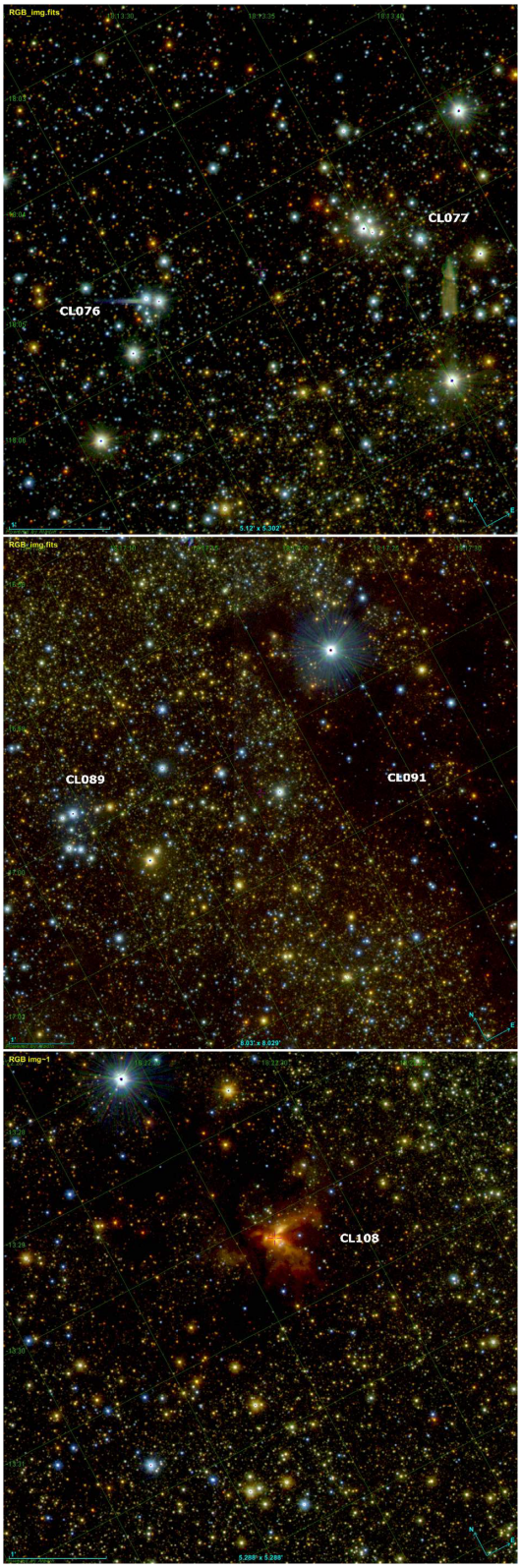

Figure 2. VVVX JHK_S composite colour images of some open cluster candidates. The field of view is 5×5 arcmin^2.

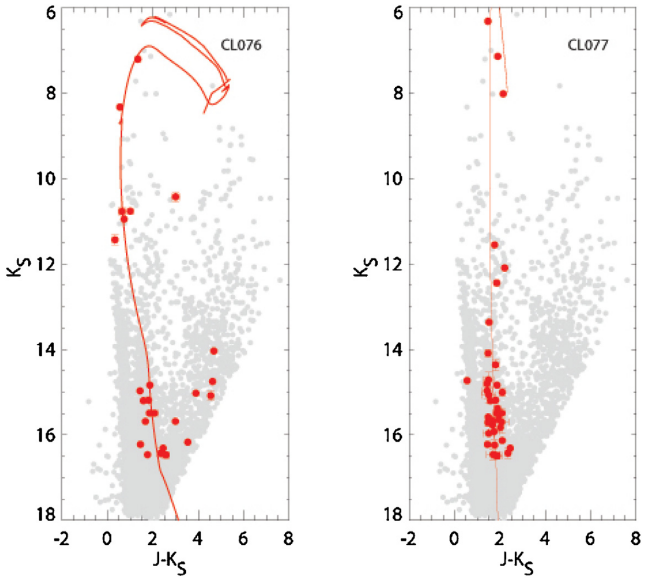

Figure 3. The VVVX CL076 and CL077 K_S versus $(J - K_S)$ diagram, with most probable cluster members (red large circles) overplotted (see text). The solid red lines are best-fitting solar isochrones of 32 and 10 Myr, respectively, taken for Padova database.

as the proper motion of the cluster. Then, only the parallaxes with errors less than 20 per cent are selected and used to calculate the median parallax and its standard deviation (Col: 8 and 9 of Table B1). No correction of parallax zero-point is performed (Lindegren et al. 2018). Using the TOPCAT implementation of Bailer-Jones (2015), Astraatmadja & Bailer-Jones (2016) and Luri et al. (2018) method we calculated 'the best estimate of distance using the Exponentially Decreasing Space Density prior' and 'the 5th and 95th percentile confidence intervals'. The 'best estimate' value is consider as the distance to the cluster, while the standard deviation of the 5th and 95th values is taken as the error of the determination.

It is hard to compare the obtained distances, because there is no data in the literature for our objects. Indirectly, we can compare some kinematic distance estimates when the cluster candidate is projected close to an H II region. For example, the calculated *Gaia* distance of 2385 pc for VVVX CL038 is in reasonable agreement with the kinematic distance of 2024 pc of the associated H II region WRAY16-205 (Stanghellini, Shaw & Villaver 2008). Nevertheless, we caution that such calculated distances should be taken as preliminary.

We have also collected *K*-band spectra of 3 and 2 stars for VVVX CL010 and CL011, respectively, using the IR spectrograph and imaging camera SofI in long-slit mode, mounted on the ESO New Technology Telescope (NTT) .[5] The instrument set-up give a resolution of $R = 2200$, and the total exposure times were 900 and 1200 s. The reduction procedure for the spectra is described in Chené et al. (2012). The equivalent widths (EWs) were measured from the continuum-normalized spectra using the IRAF[6] task SPLOT.

Fig. 5 shows the continuum-normalized spectra, all clearly exhibited characteristic features of cool stars, such as Na I (2.21 μm);

[5]Based on observations gathered with ESO programme 0101.C-0519(A).
[6]IRAF is distributed by the National Optical Astronomy Observatory, which is operated by the Association of Universities for Research in Astronomy (AURA) under cooperative agreement with the National Science Foundation.

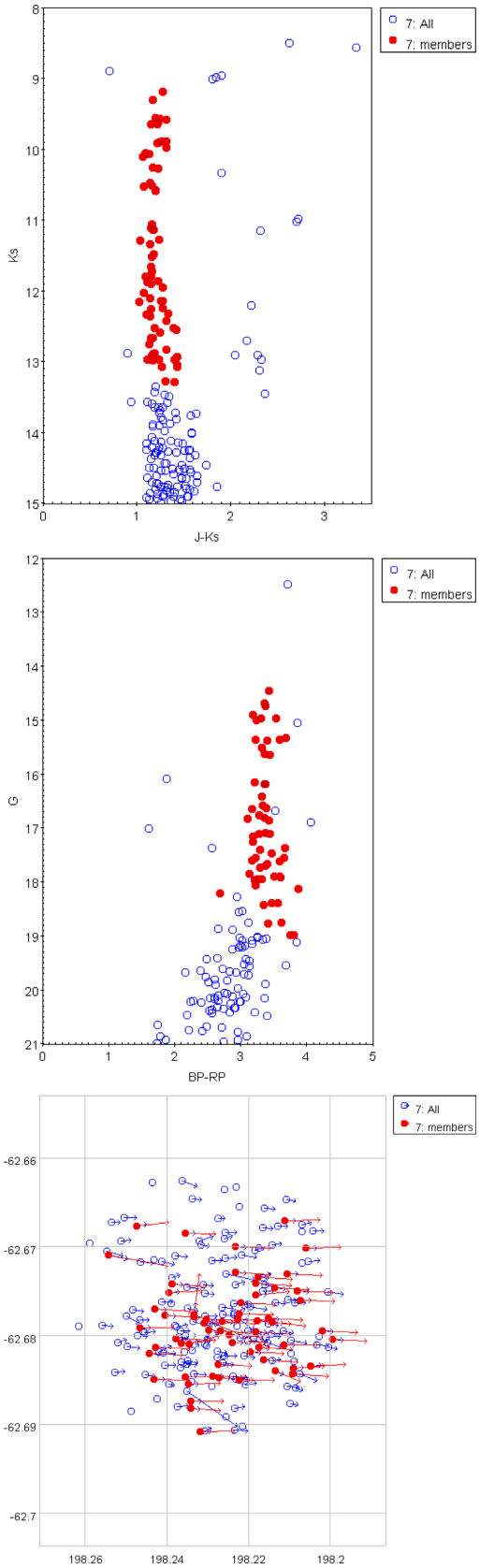

Figure 4. The VVV and *Gaia* DR2 colour–magnitude and proper motion diagrams with sky vectors overplotted for known open cluster Danks 2. Blue open circles are all stars in the selected area, the red solid ones stand for most probable cluster members. The proper motion vectors are scaled by a factor of 2 for visibility.

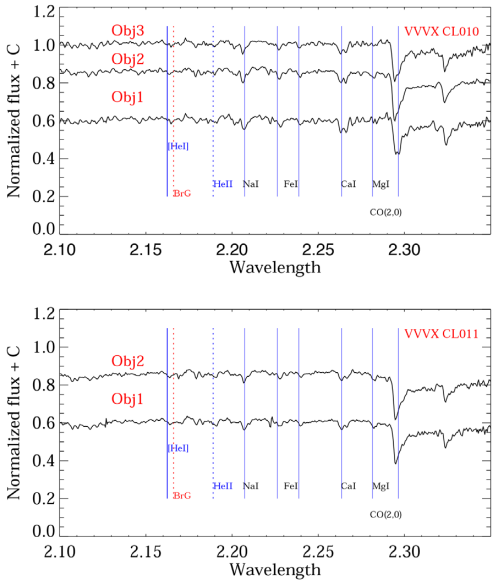

Figure 5. SofI low-resolution spectra of VVVX CL010 and CL011.

Ca I (2.26 μm) atomic line blends, and the first band-head of CO (2.29 μm). Following Borissova et al. (2014) and using the EWs of these three lines and Frogel et al. (2001) calibration we calculated the mean metallicity of [Fe/H] $= -0.39 \pm 0.06$ for CL010 and [Fe/H] $= -0.02 \pm 0.11$ for CL011.

Some parameters of these stars are measured in the *Gaia* DR2 catalogue and are tabulated in Table 1. To test $T_{\rm eff}$ as a proxy of distance, we obtained the spectral types for every star by comparing the *Gaia* temperature with the Straizys & Kuriliene (1981) Sp. Type versus temperature calibration, and then the individual extinctions and distance moduli are calculated by spectroscopic parallaxes using the intrinsic colours and luminosities, again from Straizys & Kuriliene (1981). Thus, the distance moduli to CL010 and Cl011, calculated as a mean value of the individual measurements are $(M - {\rm m})_0 = 12.61 \pm 1.07$ (3.43 kpc) and $(M - {\rm m})_0 = 12.01 \pm 0.61$ (2.56 kpc), respectively. A comparison with the *Gaia* distances given in Table B1 shows good agreement. Therefore, in some cases, when we have poorly measured *Gaia* parallaxes, but individual *Gaia* temperatures, it is still possible to estimate the distances using spectroscopic parallaxes.

4 THE CATALOGUE

We identified 120 new candidate star clusters or stellar groups, listed in Table A1. The first column gives the identification, followed by the equatorial coordinates of the centre determined by eye, eyeball measured apparent cluster radius in arcsec, the name of the corresponding VVVX tile and some comments about the nature of the object such as: presence or absence of nebulosity or H II region around the cluster, known nearby infrared, radio and X-ray sources, young stellar objects (YSO), outflow candidates and masers, taken from the SIMBAD database (http://simbad.u-strasbg.fr/simbad/).

During the visual inspection we recovered 69 known star clusters, mainly from the lists of Bica et al. (2003), Mercer et al. (2005) and Solin, Ukkonen & Haikala (2012), as well as some clusters from WEBDA[7] (Dias et al. 2002) database. These are not all known

[7]http://www.univie.ac.at/webda/

Table 1. Parameters of stars with spectra.

Name	α(2000) °	δ(2000) °	π mas	$\mu_\alpha \cos\delta$ mas	μ_δ mas	Gmag mag	$T_{\rm eff}$ K	Sp type	J mag	H mag	K_S mag	$E(J-K)$ mag	Distance kpc
CL010													
Obj1	192.66456	−64.91643	0.0092 ± 0.056	− 6.202 ± 0.076	0.144 ± 0.070	13.47 ± 0.001	3849.86	M0	9.79 ± 0.03	8.70 ± 0.05	8.24 ± 0.03	0.92	2.31
Obj2	192.66222	−64.91845	0.1428 ± 0.109	− 5.832 ± 0.151	0.233 ± 0.136	12.93 ± 0.003	3296.00	M5	8.73 ± 0.03	7.60 ± 0.02	7.10 ± 0.02	0.99	3.99
Obj3	192.65980	−64.92115	0.0624 ± 0.056	− 6.280 ± 0.076	−0.707 ± 0.070	14.38 ± 0.001	3823.60	M1	10.69 ± 0.03	9.56 ± 0.04	9.14 ± 0.02	0.88	3.98
CL011													
Obj1	192.81099	−60.59321	0.4624 ± 0.037	− 14.310 ± 0.045	−1.730 ± 0.048	11.80 ± 0.000	4048.41	K6	9.61 ± 0.03	8.89 ± 0.03	8.70 ± 0.02	0.31	3.00
Obj2	192.80710	−60.59457	0.3658 ± 0.062	− 6.740 ± 0.080	−0.260 ± 0.082	11.52 ± 0.002	3669.00	M3	8.29 ± 0.02	7.28 ± 0.04	6.94 ± 0.02	0.68	2.14

Figure 6. Distribution of the detected objects with measured cluster radius (given in arcsec). The red colour stands for young/embedded clusters, while the blue one is for open ones. The second panel shows know clusters in the VVVX area.

clusters in the VVVX area, many of optically visible clusters [for example those from Kharchenko et al. (2013)] are not taken in consideration. Another 13, previously unknown candidates are in common with Lucas et al. (in preparation) catalogue. All these objects are removed from the catalogue presented here. Finally, Ryu & Lee (2018) published a WISE catalogue of 923 new star cluster candidates. Comparison shows that we have seven common candidates. The VVVX cluster candidates CL065; CL070; CL073; CL074; CL084; CL097 and CL120 are matched within 20 arcsec radius with Ryu670; Ryu657; Ryu687; Ryu664; Ryu715; Ryu711; Ryu796, respectively. Since the Ryu & Lee (2018) catalogue was published after this paper was submitted to the journal, we consider these objects simultaneously discovered and did not remove them from our list, as in the case of previous catalogues.

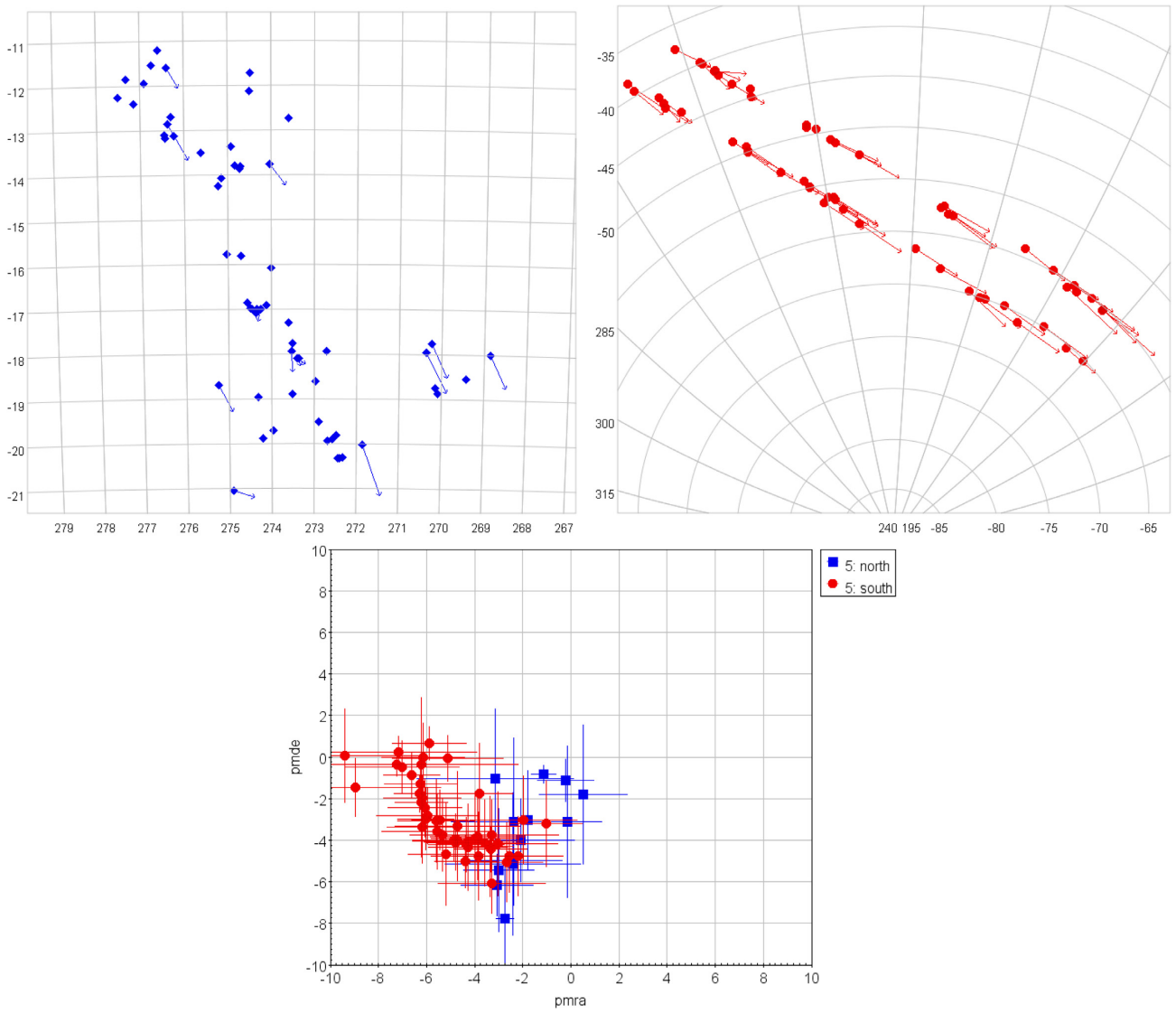

Figure 7. The diagram of mean proper motions of the cluster candidates. The blue squares are for the candidates projected in North disc VVVX area, while red circles stand for the Southern part. The proper motion vectors are scaled by a factor of 2 for visibility.

The preliminary analysis, based only on the appearance on the VVVX images, shows two general groups: 53 per cent (64 objects) have the typical appearance of open clusters and the rest of the sample (56 objects) are projected on H II regions, bubbles, nebulosity or around some early OB stars, YSOs and IR sources.

The cluster radii were measured by eye on the VVVX K_S tiles. This method was preferred over automated algorithms, in order to include objects that are not resolved into stars. The area around cluster candidates is smoothed and the density contours are overplotted with the lower limit of the contour equal to the density of comparison field. The normalized histogram of the number of star clusters versus radius is shown in Fig. 6. The sample was divided by two: embedded/young clusters (red colour) and open cluster candidates (blue colour). The Gaussian distribution gives the mean radius of the young clusters sample of 18.5 $\pm$ 9 arcsec, while the open cluster sample is centred on 57 $\pm$ 30 arcsec. For comparison, the Gaussian distribution of the known infrared clusters in the investigated VVVX area (see previous paragraph) is centred on 62 $\pm$ 47 arcsec. Thus, in this study, we are adding the fainter and compact (with small angular sizes) new candidates. This looks very similar to the size distribution plot for the clusters found by visual inspection of the GPS/VVV area (Froebrich et al. 2017). The small sizes suggest that the clusters are distant, but the sample could be biased and further investigation is necessary to confirm or reject such suggestion.

Using the information from Table 1 (see previous paragraph) we can derive some preliminary relations from the new sample of cluster candidates. In Fig. 7, left and middle part, we overplot the sky proper motion vectors, while the right panel shows the proper motion diagram. The blue squares and red circles represent the cluster candidates projected on the North and South VVVX disc area. As can be seen from the figure, in general the clusters follow the disc motion (with exception of CL049, 056, 080, 089 and 103). This is more notable in the South disc area, at higher Galactic

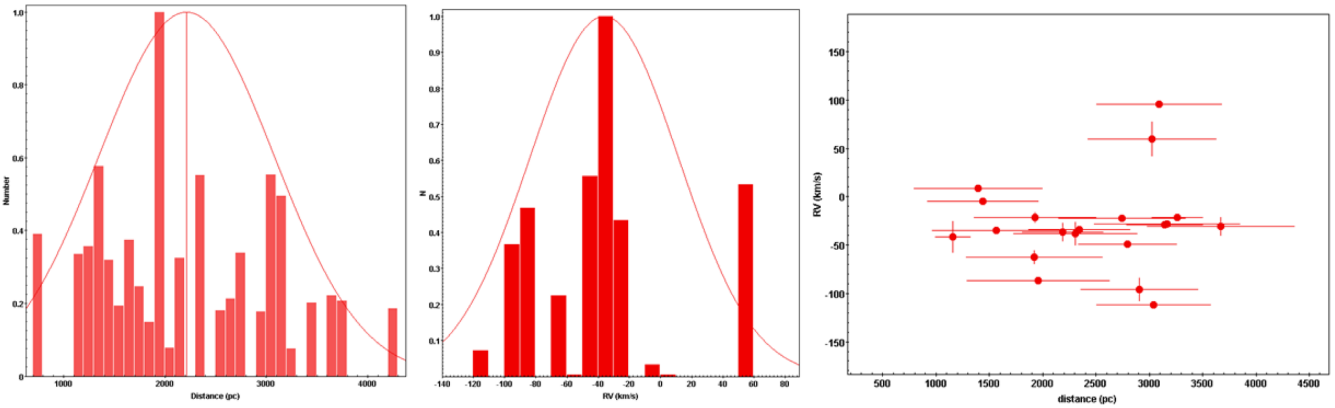

Figure 8. The histograms of distance and radial velocity distribution. The right panel shows RV versus distance relation. The solid lines are Gaussian distribution.

latitudes, where the distribution seems more homogeneous. The last panel shows a clear concentration of the candidates towards the lower left part, where the galactic disc stars are projected.

Fig. 8 illustrates the mean normalized distances and radial velocities of the cluster candidates, taking in consideration the corresponding errors. The distance distribution seems complex, with several groups around 1.3; 2.3 and 3.1 kpc. The mean value of the sample is 2.21 ± 0.86 kpc, calculated as a peak of the Gaussian distribution. Thus, *Gaia* DR2 distances can be used up to 3.5–4 kpc, but most of the clusters are closer than 2 kpc. The radial velocities are distributed around $R_V = -36 \pm 47\,\mathrm{km\,s^{-1}}$. A very weak correlation (9 per cent) between radial velocities and distances is found, but this could be selection, small sample effect. Again, these values should be taken as preliminary and used with caution.

5 SUMMARY

In this work we report a catalogue of 120 new infrared clusters and stellar groups projected in the disc area covered by the ongoing 'VISTA Variables in the Vía Láctea eXtended (VVVX)' ESO Public Survey. The search is performed by visual inspection on the pipeline processed and calibrated K_S-band tile images. The initial list of candidates is then validated using the composite JHK_S colour images, K_S versus $(J - K_S)$ colour–magnitude diagrams and *Gaia* DR2 proper motions. A smaller proportion of embedded candidates is detected in comparison with previous VVV searches, as would be expected given that much of the area searched is slightly further from the Galactic equator. The smaller number density of candidates is explained by the fact that the area covered by this new search (the outer part of the Galactic disc) is significantly less crowded and reddened than that of the previous search. In general, the clusters follow the disc motion. The *Gaia* DR2 distances are estimated up to 3.5–4 kpc, but most of the clusters are closer than 2 kpc.

ACKNOWLEDGEMENTS

We gratefully acknowledge data from the ESO Public Survey programme ID 198.B-2004 taken with the VISTA telescope, and products from the Cambridge Astronomical Survey Unit (CASU). This work has made use of data from the European Space Agency (ESA) mission *Gaia* (https://www.cosmos.esa.int/gaia), processed by the *Gaia* Data Processing and Analysis Consortium (DPAC, https://www.cosmos.esa.int/web/gaia/dpac/consortium). Funding for the DPAC has been provided by national institutions, in particular the institutions participating in the *Gaia* Multilateral Agreement. Support is provided by the Ministry for the Economy, Development and Tourism, Programa Iniciativa Cientica Milenio grant IC120009, awarded to the Millennium Institute of Astrophysics (MAS). JB and RK thank ESO for the financial support during their 2018 January visit. ANC's work is supported by the Gemini Observatory, which is operated by the Association of Universities for Research in Astronomy, Inc., on behalf of the international Gemini partnership of Argentina, Brazil, Canada, Chile, and the United States of America. SRA thanks the support by the FONDECYT Iniciación project No. 11171025 and the CONICYT + PAI 'Concurso Nacional Inserción de Capital Humano Avanzado en la Academia 2017' project PAI 79170089. JA-G also acknowledges support by FONDECYT Iniciación 11150916. MH acknowledges support by the BASAL Centre for Astrophysics and Associated Technologies (CATA) through grant PFB-06. We thank anonymous referee for useful comments and suggestions.

REFERENCES

Alonso-García J. et al., 2017, ApJ, 849, L13
Astraatmadja T. L., Bailer-Jones C. A. L., 2016, ApJ, 832, 137
Bailer-Jones C. A. L., 2015, PASP, 127, 994
Barbá R. et al., 2015, A&A, 581, 120
Benjamin R. A. et al., 2003, PASP, 115, 953
Bica E. et al., 2003, A&A, 404, 223
Borissova J. et al., 2003, A&A, 411, 83
Borissova J. et al., 2011, A&A, 532, 131
Borissova J. et al., 2014, A&A, 569, 24
Borissova J. et al., 2016, AJ, 152, 74
Bressan A., Marigo P., Girardi L., Salasnich B., Dal Cero C., Rubele S., Nanni A., 2012, MNRAS, 427, 127
Camargo D., Bica E., Bonatto C., 2016, A&A, 593, A95
Chené A.-N. et al., 2012, A&A,, 545, A54
Chené A.-N. et al., 2013, A&A,, 549, 98
Chené A.-N. et al., 2015, A&A,, 584, 31
Cross N. J. G. et al., 2012, A&A,, 548, A119
Dalton G. B. et al., 2006, in SPIE Conf. Ser. Vol. 6269, p. 30
Dias W. S. et al., 2002, A&A, 389, 871
Emerson J. P. et al., 2004, in SPIE Conf. Ser. Vol. 5493, p. 401
Emerson J., McPherson A., Sutherland W., 2006, The Messenger, 126, 41

Froebrich D., et al., 2017, MNRAS, 469, 1545
Frogel J. A., Stephens A., Ramírez S., DePoy D. L., 2001, AJ, 122, 1896
Gaia Collaboration et al., 2016, A&A, 595, A1
Gaia Collaboration et al., 2018, A&A, 616, 13
Gaia Collaboration et al., 2018, A&A, 616, 1
Hervé A., Martins F., Chené A.-N., Bouret J.-C., Borissova J., 2016, New Astron., 45, 84
Irwin M. J. et al., 2004, in SPIE Conf. Ser.Vol. 5493, p. 411
Ivanov V. D . et al., 2002, A&A, 394, L1
Ivanov V. D., Kurtev R., Borissova J., 2005, A&A, 442, 195
Ivanov V. D. et al., 2017, A&A, 600, 112
Kharchenko N. V. et al., 2013, A&A, 558, 53
Lindegren L. et al., 2018, A&A, 616, 2
Lucas P. W., et al., 2008, MNRAS, 391, 136
Luri X. et al., 2018, A&A, 616, 9
Medina N. et al., 2018, ApJ, 864, 11
Mercer E. P. et al., 2005, ApJ, 635, 560
Minniti D. et al., 2010, New Astron., 15, 433
Minniti D. et al., 2011, A&A, 527, 81
Minniti D. et al., 2017a, ApJ, 849, 24
Minniti D. et al., 2017b, RNAAS, 1, 16
Minniti D., Alonso-García J., Pullen J., 2017c, RNAAS, 1, 54
Moni-Bidin C. et al., 2011, A&A, 535, 33
Morales E. F. E . et al., 2013, A&A, 560, 76
Navarro Molina C. et al., 2016, MNRAS, 462, 1180
Pfalzner S. et al., 2016, A&A, 586, 68
Portegies Zwart S. F., McMillan S. L. W., Gieles M., 2010, ARA&A, 48, 431
Ramírez Alegría S. et al., 2014, A&A, 564, 9
Ryu J., Lee M. G., 2018, ApJ, 856, 152
Saito R. K. et al., 2012, A&A, 537, 107
Schmeja S. et al., 2014, A&A, 568, 51
Skrutskie M. F. et al., 2006, AJ, 131, 1163
Solin O., Ukkonen E., Haikala L., 2012 A&A, 542, 3
Solin O., Haikala L., Ukkonen E., 2014, A&A, 562, 115
Stanghellini L., Shaw R. A., Villaver E., 2008, ApJ, 689, 194
Straizys V., Kuriliene G., 1981, Ap&SS, 80, 353
Wright E. L. et al., 2010, AJ, 140, 1868
Zasowski G. et al., 2013, AJ, 146, 64

APPENDIX A: VVVX CLUSTER CANDIDATES: CATALOGUE

In Table A1 are tabulated 120 new candidate star clusters or stellar groups. The first column gives the identification, followed by the equatorial coordinates of the centre determined by eye, eye-ball measured apparent cluster radius in arcsec, the name of the corresponding VVVX tile and some comments about the nature of the object.

Table A1. VVVX cluster candidates: catalogue.

Name	α(2000) °	δ(2000) °	Radius arcsec	VVVX tile	Comments
VVVX CL001	180.380770	−65.137202	18	e0730	Very faint, embedded group of stars
VVVX CL002	180.397080	−65.126113	20	e0730	Very faint, embedded group of stars
VVVX CL003	184.276940	−60.220145	29	e0814	Small open cluster
VVVX CL004	184.307420	−60.303649	55	e0814	Open cluster
VVVX CL005	184.324520	−60.242285	45	e0814	Small reddened open cluster
VVVX CL006	185.437370	−65.356478	55	e0732	O9 star+group of bright stars
VVVX CL007	187.473880	−60.114671	120	e0815	Open cluster
VVVX CL008	190.768300	−60.437844	34	e0816	Faint, embedded group of stars
VVVX CL009	191.765130	−60.072564	66	e0816	Several bright stars, open cluster, IRAS 12441-5947
VVVX CL010	192.658350	−64.916684	38	e0734	Concentrated open cluster?
VVVX CL011	192.800920	−60.592911	55	e0817	Several bright stars, open cluster
VVVX CL012	196.764630	−59.841214	62	e0818	Several bright stars, open cluster
VVVX CL013	198.576150	−65.840076	50	e0735	Several bright stars, open cluster
VVVX CL014	202.949120	−64.935656	55	e0737	Open cluster
VVVX CL015	203.442400	−59.141331	31	e0821	Several bright stars, open cluster
VVVX CL016	207.530690	−65.007603	12	e0738	Very faint, weak nebula, group of stars
VVVX CL017	208.820520	−65.056893	66	e0738	Open cluster
VVVX CL018	211.590200	−64.731412	23	e0739	Small group, dissolved?
VVVX CL019	217.911420	−58.051811	145	e0826	Open cluster
VVVX CL020	218.723750	−63.222653	36	e0742	Open cluster
VVVX CL021	218.823650	−57.981169	40	e0826	Several bright stars, open cluster
VVVX CL022	219.642140	−57.257272	80	e0826	Open cluster
VVVX CL023	220.166310	−57.441524	105	e0827	Open cluster
VVVX CL024	224.245480	−61.592499	28	e0744	Open cluster
VVVX CL025	234.033390	−52.575296	59	e0833	Open cluster
VVVX CL026	234.949620	−59.136058	68	e0748	B8Ib+group
VVVX CL027	237.487450	−57.608643	70	e0749	Group of stars
VVVX CL028	237.510440	−51.179911	85	e0835	Open cluster
VVVX CL029	238.130460	−50.768071	125	e0835	Open cluster
VVVX CL030	238.709700	−56.558402	67	e0750	Open cluster
VVVX CL031	238.944100	−56.279803	140	e0750	OB star+group of stars
VVVX CL032	239.836430	−56.233403	51	e0750	B9 star + group of stars
VVVX CL033	240.062400	−49.524395	13	e0836	Faint, weak nebula, group of stars, 2MASX J16001524-4931255
VVVX CL034	240.695290	−56.720018	37	e0750	Open cluster
VVVX CL035	241.357520	−48.991222	38	e0837	Very red group of stars, radio source [CAB2011] G332.40+2.46
VVVX CL036	241.423240	−49.191992	17	e0837	Embedded group+ Maser: Caswell OH 332.295+02.280?+YSO: 2MASS J16054183-4911294
VVVX CL037	242.630320	−54.937447	8	e0752	Embedded faint group + YSO [MHL2007] G328.9716-02.4664 1
VVVX CL038	242.670130	−54.961111	21	e0752	Group in H II region: WRAY 16-205
VVVX CL039	243.306690	−54.287039	22	e0752	Open cluster, concentrated
VVVX CL040	246.636880	−52.874636	60	e0754	Compact group of 2MASS variable stars
VVVX CL041	247.898680	−44.174854	33	e0841	Open cluster
VVVX CL042	248.132730	−44.924463	64	e0841	Embedded +Variable Star of FU Ori type: V∗ V346 Nor
VVVX CL043	250.190380	−43.120268	89	e0843	Open cluster
VVVX CL044	250.562580	−49.889192	72	e0756	Open cluster
VVVX CL045	250.705140	−50.061132	75	e0756	Open cluster
VVVX CL046	250.706130	−49.467184	50	e0757	GC?
VVVX CL047	251.500630	−41.766043	59	e0844	Open cluster
VVVX CL048	251.723100	−41.233356	10	e0844	Small group in cloud: MSX6C G343.0500+02.6094
VVVX CL049	251.860180	−41.244139	15	e0844	Group around Emission-line Star: [OSP2002] BRC 82 11
VVVX CL050	252.328640	−48.592074	17	e0758	Concentrated group around Object of unknown nature: XZLJ Nor 111
VVVX CL051	253.042590	−40.065037	81	e0845	Open cluster
VVVX CL052	253.294640	−39.836432	31	e0846	Open cluster
VVVX CL053	255.785070	−37.520748	43	e0848	Open cluster
VVVX CL054	257.723300	−43.705101	30	e0762	Embedded group
VVVX CL055	259.483430	−42.657861	38	e0763	Open cluster
VVVX CL056	259.499020	−42.094804	86	e0764	Open cluster
VVVX CL057	259.780310	−41.405093	12	e0764	Concentrated group
VVVX CL058	262.414960	−39.466213	94	e0766	Open cluster
VVVX CL059	262.844920	−38.469595	100	e0766	Open cluster
VVVX CL060	268.852770	−18.000075	55	e0982	Open cluster

Table A1 *– continued*

Name	α(2000) °	δ(2000) °	Radius arcsec	VVVX tile	Comments
VVVX CL061	269.430960	−18.542233	31	e0975	Group of stars in Interstellar matter: [GMG2004] 85
VVVX CL062	270.094130	−18.869869	18	e0975	Embedded cluster? Too big to be single YSO: [MJR2015] 113
VVVX CL063	270.144320	−18.754833	29	e0975	Group in H II region: MSX6C G010.5067+02.2285
VVVX CL064	270.249460	−17.749453	69	e0975	Open cluster
VVVX CL065	270.369110	−17.946281	65	e0975	Open cluster
VVVX CL066	271.856700	−20.028048	36	e0961	Open cluster
VVVX CL067	272.318750	−20.312052	47	e0954	Young cluster part of W31?
VVVX CL068	272.405310	−20.320490	21	e0954	Small group in Bubble [CWP2007] CN 145
VVVX CL069	272.436630	−20.336289	53	e0954	Group in H II region: [L89b] 10.190-00.426
VVVX CL070	272.482890	−19.806053	24	e0954	Group in Bubble: [SPK2012] MWP1G010670-002100S
VVVX CL071	272.579460	−19.902798	22	e0954	Small group in H II region: [AAJ2015] G010.630-00.338
VVVX CL072	272.678330	−19.942037	14	e0954	Group in H II region: HRDS G010.638-00.434
VVVX CL073	272.713320	−17.931154	28	e0962	Group in H II region: GAL 012.42+00.50
VVVX CL074	272.884650	−19.510605	28	e0954	Small group around YSO: IRAS 18085-1931
VVVX CL075	272.971860	−18.605660	10	e0955	Small group in H II region: [KC97c] G011.9+00.0
VVVX CL076	273.354540	−18.092123	17	e0955	Concentrated group
VVVX CL077	273.396040	−18.096607	53	e0955	Concentrated group close to CL076+WR, binary cluster?
VVVX CL078	273.504900	−18.891444	22	e0955	Young cluster in H II region GRS G011.94 -00.62
VVVX CL079	273.510870	−17.758839	20	e0955	Group in Bubble: [SPK2012] MWP1G012930-000811
VVVX CL080	273.527110	−17.934716	19	e0955	Small group around B0V star [MCF2015] 13, neb, concentrated
VVVX CL081	273.587430	−12.742477	20	e0973	Small group around YSO: MSX6C G017.3765+02.2512
VVVX CL082	273.601520	−17.293137	18	e0956	Group in Bubble: [SPK2012] MWP1G013382+000659
VVVX CL083	273.955800	−19.703903	23	e0947	Small very red group, neb.
VVVX CL084	274.006270	−16.085923	15	e0964	Neb, IR: IRAS 18131-1606
VVVX CL085	274.006350	−16.085481	17	e0964	Group of stars, neb., IR source
VVVX CL086	274.040020	−13.755454	49	e0972	Open cluster
VVVX CL087	274.111360	−16.913282	35	e0956	Open cluster
VVVX CL088	274.208750	−19.889306	10	e0947	Small group around YSO: MSX6C G011.3757-01.6770
VVVX CL089	274.247920	−16.999377	48	e0956	Open cluster
VVVX CL090	274.312720	−18.954494	132	e0948	Open cluster
VVVX CL091	274.342440	−16.999377	25	e0956	Young cluster or dust window
VVVX CL092	274.361490	−17.092749	10	e0956	Embedded group around YSO:[PW2010] 48
VVVX CL093	274.461220	−16.999192	10	e0956	Embedded, compact group in H II region: MSX6C G014.0329-00.5155
VVVX CL094	274.477580	−11.725361	13	e0973	Second small group of stars close to BDS9, sub-cluster?
VVVX CL095	274.481180	−16.975518	10	e0956	Small group around YSO: SSTGLMA G014.0632-00.5199
VVVX CL096	274.492270	−12.123610	16	e0973	Small group around YSO: IRAS 18151-1208
VVVX CL097	274.561750	−16.851552	34	e0956	Neb, YSOs, bubbles, IR
VVVX CL098	274.696620	−15.814823	20	e0957	Group in H II region: IRAS 18159-1550
VVVX CL099	274.709510	−13.815189	15	e0965	Small group in H II region: MSX6C G016.9512+00.7806, close to M16, sub-cluster?
VVVX CL100	274.717510	−13.859019	16	e0965	Four bright stars, very compact, part of M16, RSG?
VVVX CL101	274.827630	−13.794123	78	e0965	Group in M16 (NGC 6611) region, sub-cluster?
VVVX CL102	274.916667	−13.362500	11	e0966	Group in H II region: MSX6C G017.4507+00.8118
VVVX CL103	274.923010	−21.059604	32	e0940	Group
VVVX CL104	275.026400	−15.778958	10	e0957	Small group in H II region: [SPE2008b] IRAS 18171-1548 VLA 1
VVVX CL105	275.147920	−14.070781	13	e0965	Embedded source in H II region: MSX6C G016.9261+00.2854
VVVX CL106	275.230480	−14.258462	10	e0965	Small group around YSO: 2MASS J18205529-1415306
VVVX CL107	275.250670	−18.696785	48	e0948	Open cluster
VVVX CL108	275.611970	−13.504312	45	e0966	Young cluster in SFR: RAFGL 2136
VVVX CL109	276.228570	−13.120082	35	e0950	GC?
VVVX CL110	276.294290	−12.704624	18	e0959	Small group in H II region: [ABB2014] WISE G018.657-00.057
VVVX CL111	276.365960	−12.853166	77	e0959	Open cluster
VVVX CL112	276.389290	−11.588813	20	e0967	Open cluster
VVVX CL113	276.427310	−13.172107	52	e0950	Group in H II region: [CKW87] 182253.2-131203
VVVX CL114	276.451510	−13.108666	11	e0959	Small group around YSO: IRAS 18229-1308
VVVX CL115	276.594240	−11.202625	20	e0967	Group around emission line stars: LS IV -11 19
VVVX CL116	276.738040	−11.535798	10	e0967	Compact group around YSO: IRAS 18241-1134
VVVX CL117	276.910160	−11.945382	12	e0960	Compact group in H II region: [WBH2005] G019.608-0.237
VVVX CL118	277.149220	−12.407517	10	e0960	Compact group in H II region: IRAS 18257-1226
VVVX CL119	277.312510	−11.839633	10	e0960	Group in H II region: MSX6C G019.8817-00.5347
VVVX CL120	277.511290	−12.257561	20	e0960	Group in bubble: [SPK2012] MWP1G019605-009038

APPENDIX B: VVVX CLUSTER CANDIDATES: PARAMETERS

In Table B1 are tabulated the candidate star clusters with reliable *Gaia* DR2 parameters. The first column gives the identification, followed by the equatorial coordinates of the centre, median proper motion and parallax, as well as the calculated distance and radial velocity, with corresponding errors.

Table B1. VVVX cluster candidates: parameters.

Name	α(2000) °	δ(2000) °	$\mu_\alpha \cos\delta$ mas	Err $\mu_\alpha \cos\delta$ mas	μ_δ mas	Err μ_δ mas	π mas	Err π mas	Dis kpc	Dis 5% kpc	Dis 95% kpc	RV km s^{-1}	Err RV km s^{-1}	E(BP-RP) mag	Err E(BP-RP) mag
VVVX CL003	184.276940	−60.220145	−6.2048	4.0251	−0.3767	3.2011	0.4006	0.2471	1568	1142	2838	−35.24	3.26	0.63	0.40
VVVX CL004	184.307420	−60.303649	−5.8743	1.5290	0.6543	0.8239	0.2025	0.0713	3166	2543	4465	−27.99	6.44	0.80	0.21
VVVX CL005	184.324520	−60.242285	−9.3827	3.2809	0.0499	2.2410	0.4337	0.1749	1710	1299	2855			0.78	0.43
VVVX CL006	185.437370	−65.356478	−5.1240	2.3100	−0.0600	1.1000	0.3605	0.0772	2346	1921	3266	−34.39	0.52	0.64	0.40
VVVX CL007	187.473880	−60.114671	−7.1671	3.2500	0.2260	0.7475	0.1850	0.0530	3670	3010	4958	−30.71	19.12	0.82	0.26
VVVX CL009	191.765130	−60.072564	−6.1444	1.7354	−0.0144	1.6379	0.5445	0.2224	1439	1077	2555	−4.85	2.20	0.98	0.63
VVVX CL010	192.658350	−64.916684	−7.2231	1.2559	−0.3623	0.5297	0.2183	0.0534	3409	2811	4584			0.65	0.36
VVVX CL011	192.800920	−60.592911	−8.9430	3.5489	−1.4580	1.3995	0.4141	0.0683	2186	1832	2907	−36.81	18.53	0.63	0.38
VVVX CL012	196.764630	−59.841214	−7.0325	2.3901	−0.4942	1.2560	0.2470	0.0646	3024	2466	4174	59.38	34.84	1.01	0.21
VVVX CL013	198.576150	−65.840076	−6.6136	1.1734	−0.8688	1.1200	0.1952	0.0303	4257	3656	5297			0.63	0.13
VVVX CL014	202.949120	−64.935656	−6.2479	1.4922	−1.3088	0.8171	0.2526	0.1972	1933	1425	3282			0.79	0.18
VVVX CL015	203.442400	−59.141331	−6.2920	1.0532	−1.7710	0.8923	0.2979	0.0193	3260	2980	3651	−21.63	3.85	0.75	0.20
VVVX CL017	208.820520	−65.056893	−6.1841	1.5941	−1.9572	1.0552	0.2501	0.0589	3092	2544	4199	95.32	1.10	0.69	0.21
VVVX CL018	211.590200	−64.731412	−5.6120	1.6243	−3.0585	1.9840	0.2964	0.0315	3143	2763	3768	−29.33	0.89	0.64	0.06
VVVX CL019	217.911420	−58.051811	−6.0215	1.1670	−2.9814	1.4978	0.2657	0.0456	3195	2697	4131			1.25	0.39
VVVX CL020	218.723750	−63.222653	−6.2019	1.0804	−2.1719	2.6371	0.9905	1.1153	795	480	2224			1.07	0.16
VVVX CL021	218.823650	−57.981169	−6.1757	1.4781	−3.3479	1.7196	0.3039	0.0834	2527	2034	3621			1.35	0.11
VVVX CL022	219.642140	−57.257272	−6.0517	1.5384	−2.4212	1.4175	0.8489	0.0980	1158	998	1458	−41.37	32.49	1.12	0.22
VVVX CL023	220.166310	−57.441524	−5.9583	2.1346	−2.8311	1.3637	0.3710	0.1483	1925	1477	3096	−21.68	10.59	1.15	0.25
VVVX CL024	224.245480	−61.592499	−5.4323	1.1612	−3.0226	1.4221	0.2279	0.0997	2660	2083	3962			0.87	0.21
VVVX CL025	234.033390	−52.575296	−4.7031	2.5805	−3.3457	2.6372	0.1983	0.0446	3781	3151	4969			0.94	0.17
VVVX CL026	234.949620	−59.136058	−4.8548	1.7112	−4.0185	0.9792	0.4375	0.3185	1394	989	2693	8.72	0.34	0.97	0.38
VVVX CL027	237.487450	−57.608643	−4.7041	1.3876	−3.9946	1.3720	0.2847	0.1872	1923	1428	3240	−62.72	13.12	0.94	0.24
VVVX CL028	237.510440	−51.179911	−5.3555	1.3411	−3.7328	1.7328						−64.80	1.58	1.11	0.38
VVVX CL029	238.130460	−50.768071	−5.5530	2.2960	−3.5770	1.8099	0.3526	0.1424	1993	1532	3176			1.37	0.07
VVVX CL030	238.709700	−56.558402	−4.7720	1.3078	−4.0830	1.3743	0.2294	0.1996	1960	1441	3328	−87.11	6.31	0.87	0.26
VVVX CL031	238.944100	−56.279803	−4.7880	1.2216	−4.1505	1.1470	0.3110	0.0526	2798	2356	3655	−49.13	0.27	0.98	0.20
VVVX CL032	239.836430	−56.233403	−4.3580	1.5724	−4.2170	1.3106	0.3185	0.1039	2309	1823	3451	−38.27	23.88	0.99	0.32
VVVX CL034	240.695290	−56.720018	−4.2690	2.2917	−4.0300	1.6007	0.2762	0.0611	2903	2393	3944	−95.56	23.94	0.93	0.03
VVVX CL038	242.670130	−54.961111	−5.1820	1.5626	−4.6810	2.4419	0.2286	0.1289	2385	1827	3720			0.72	0.08
VVVX CL039	243.306690	−54.287039	−4.2715	1.6418	−4.3275	2.0885	0.4372	0.1931	1653	1242	2827				
VVVX CL040	246.636880	−52.874636	−3.8840	1.9633	−3.8520	2.0800						−48.65	3.54	1.12	0.29
VVVX CL043	250.190380	−43.120268	−3.2785	2.7690	−3.7650	1.6912						−59.46	0.24	1.43	0.28
VVVX CL044	250.562580	−49.889192	−4.3970	1.2967	−5.0395	1.2528								1.24	0.10
VVVX CL045	250.705140	−50.061132	−3.0395	2.4861	−4.1620	2.5077	0.5739	0.1870	1460	1120	2462			1.46	0.01
VVVX CL046	250.706130	−49.467184	−3.3370	1.5034	−4.4080	1.1117								1.45	0.14
VVVX CL047	251.500630	−41.766043	−3.8320	1.9812	−4.7850	2.1367	0.2699	0.0540	3038	2529	4043	−111.89	0.51	1.23	0.28
VVVX CL049	251.860180	−41.244139	−3.7890	1.4063	−1.7590	2.4079	1.1548	1.0419	765	471	2173			0.93	0.10

Table B1 – *continued*

Name	α(2000) °	δ(2000) °	$\mu_\alpha \cos\delta$ mas	Err $\mu_\alpha \cos\delta$ mas	μ_δ mas	Err μ_δ mas	π mas	Err π mas	Dis kpc	Dis 5% kpc	Dis 95% kpc	RV km s^{-1}	Err RV km s^{-1}	E(BP-RP) mag	Err E(BP-RP) mag
VVVX CL050	252.328640	−48.592074	−3.3730	0.9842	− 4.3005	2.4106	0.3585	0.4223	1309	894	2680			1.25	0.14
VVVX CL051	253.042590	−40.065037	−3.9830	1.8397	− 3.9330	2.1836						− 87.12	24.18	1.23	0.31
VVVX CL052	253.294640	−39.836432	−2.5690	2.2240	− 4.7870	1.7466	0.4713	0.0485	2042	1791	2468			1.44	0.03
VVVX CL053	255.785070	−37.520748	−3.5670	1.5156	− 4.1120	2.0580						− 118.28	4.16	1.32	0.14
VVVX CL055	259.483430	−42.657861	−1.9610	2.2399	− 3.0390	2.1161								1.41	0.10
VVVX CL056	259.499020	−42.094804	−1.0270	1.4837	− 3.1790	2.0557	0.2695	0.0773	2740	2209	3891	− 21.96	6.59	1.30	0.19
VVVX CL057	259.780310	−41.405093	−2.6640	1.5039	− 5.0680	1.8897	0.7533	0.0419	1320	1217	2811				
VVVX CL058	262.414960	−39.466213	−2.1975	1.7054	− 4.7495	1.9031	0.4497	0.1134	1882	1503	2810			1.33	0.39
VVVX CL059	262.844920	−38.469595	−3.3055	2.2459	− 6.0655	1.4374								1.22	0.29
VVVX CL060	268.852770	−18.000075	−2.3860	2.0186	− 4.9815	1.5989	0.2806	0.1362	2198	1684	3471			1.08	0.17
VVVX CL064	270.249460	−17.749453	−2.4080	2.8298	− 5.1290	3.4491								1.15	0.35
VVVX CL065	270.369110	−17.946281	−3.0780	1.5112	− 6.1625	1.4636								1.32	0.27
VVVX CL066	271.856700	−20.028048	−2.7450	0.3543	− 7.7680	2.9813									
VVVX CL076	273.354540	−18.092123	−0.2315	1.1797	− 1.1350	1.0050	0.7011	0.3490	1141	819	2322			1.43	0.26
VVVX CL077	273.396040	−18.096607	−1.1500	0.5148	− 0.8470	0.4311								1.36	0.10
VVVX CL080	273.527110	−17.934716	−0.1565	1.4374	− 3.1130	3.6308	0.5336	0.4174	1201	829	2514			0.97	0.21
VVVX CL086	274.040020	−13.755454	−2.3780	2.5917	− 3.1320	4.0305	0.5628	0.0620	1718	1494	2116			1.35	0.10
VVVX CL089	274.247920	−16.999377	0.5210	1.8414	− 1.7870	3.3595	0.6742	0.2940	1210	886	2335			1.05	0.53
VVVX CL102	274.916667	−13.362500												1.47	0.10
VVVX CL103	274.923010	−21.059604	−3.1400	3.2674	− 1.0220	3.3342	0.8086	0.1970	1154	907	1894				
VVVX CL107	275.250670	−18.696785	−2.0890	2.2319	− 4.0075	1.9944								1.09	0.13
VVVX CL111	276.365960	−12.853166	−3.0080	1.4469	− 5.4595	2.9577									
VVVX CL112	276.389290	−11.588813	−1.7930	1.4948	− 3.0460	2.3819	0.3824	0.2343	1621	1186	2895			1.45	0.31

APPENDIX C: COMPOSITE COLOUR IMAGES OF VVVX OPEN CLUSTER CANDIDATES

Fig. C1 shows the composite colour images of VVVX open cluster candidates. The field of view is 2.5×2.5 arcmin^2, north is up, east to the left (unless specified in the image). The clusters are shown in order corresponding of Table A1. The red large circles indicate the cluster candidate approximated boundaries and are given to assist the reader to easy identification.

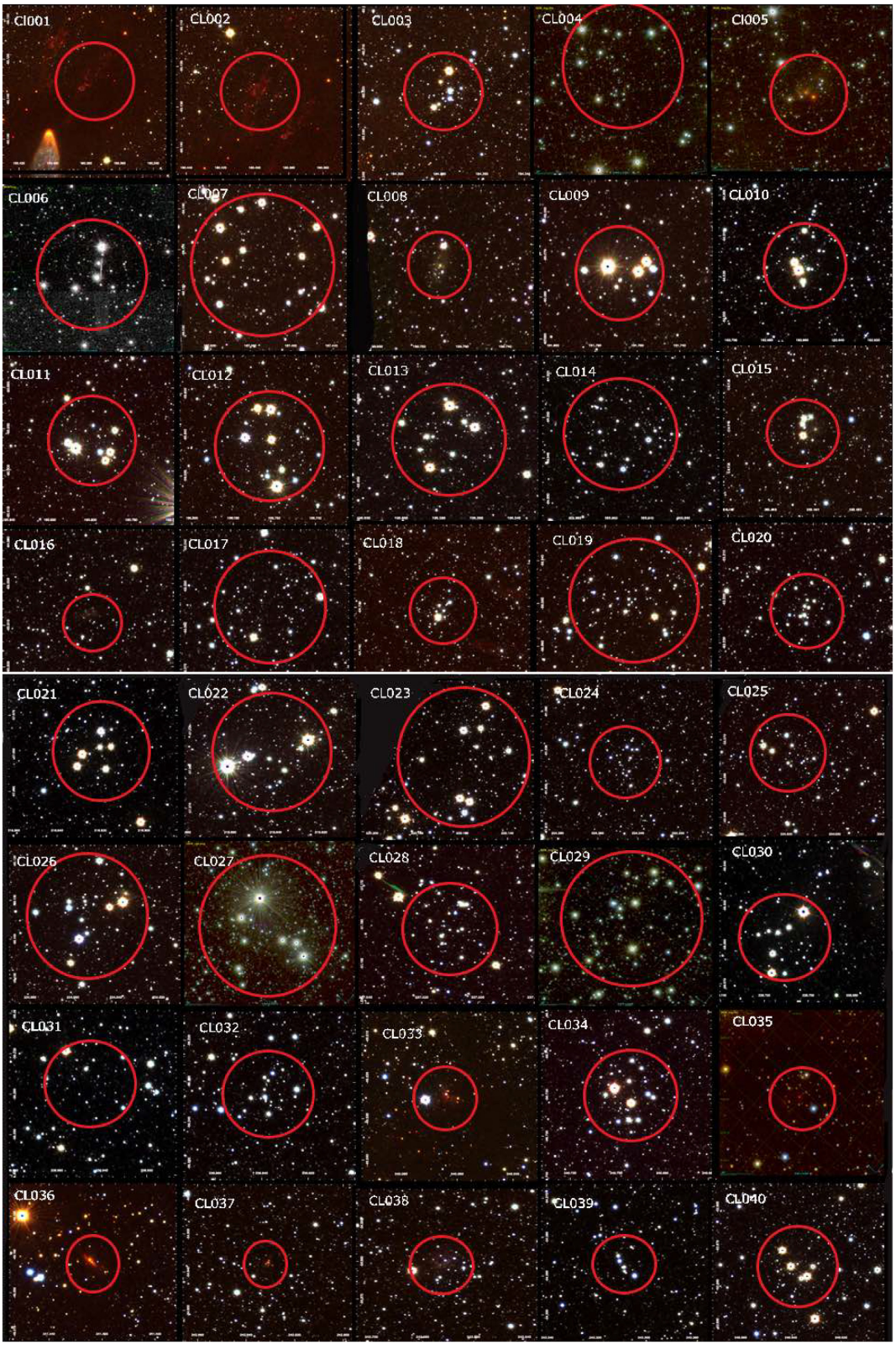

Figure C1. VVVX JHK_S composite colour images of the open cluster candidates. The field of view is 2.5×2.5 arcmin^2, north is up, east to the left.

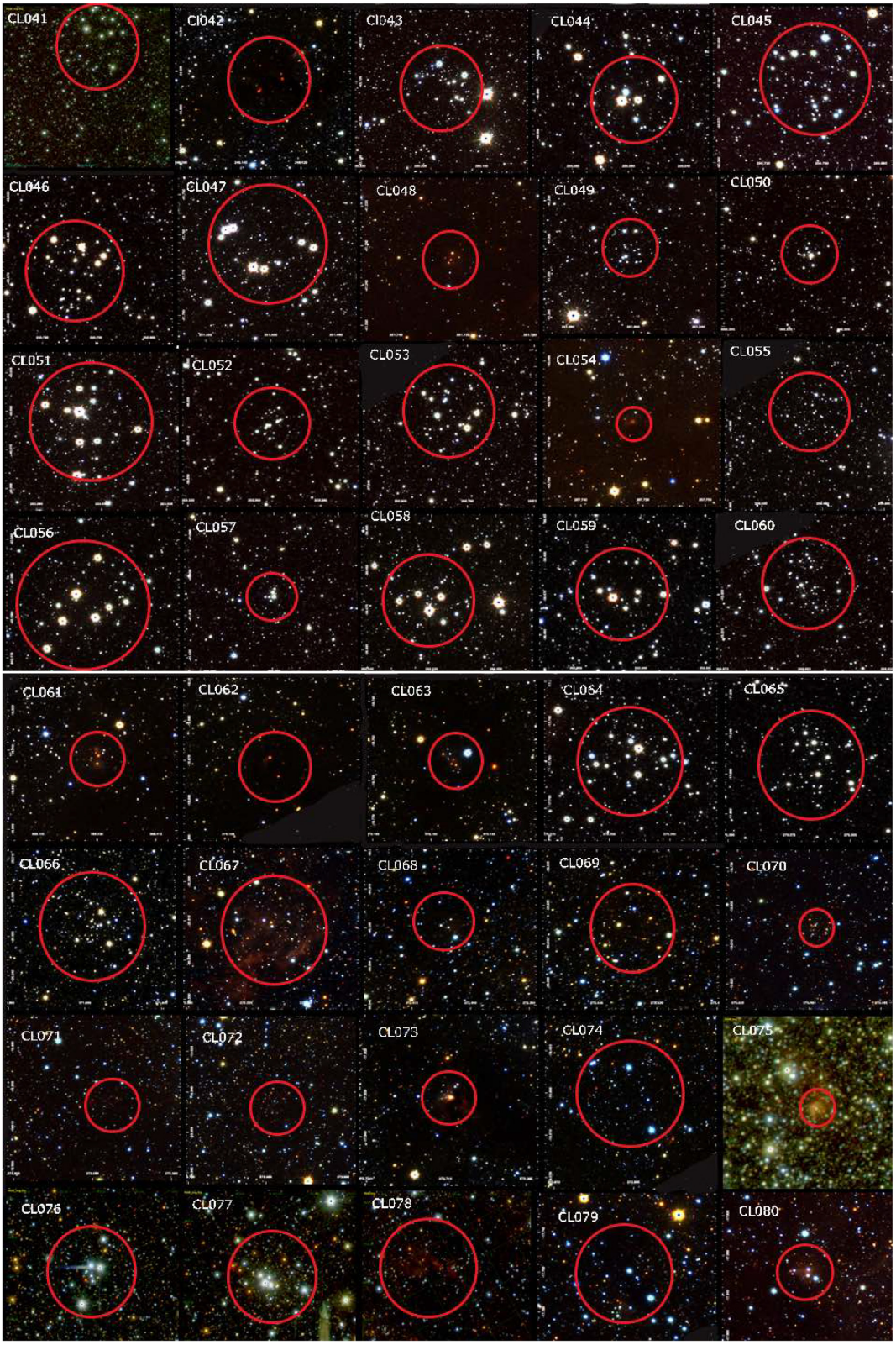

Figure C1 *continued*

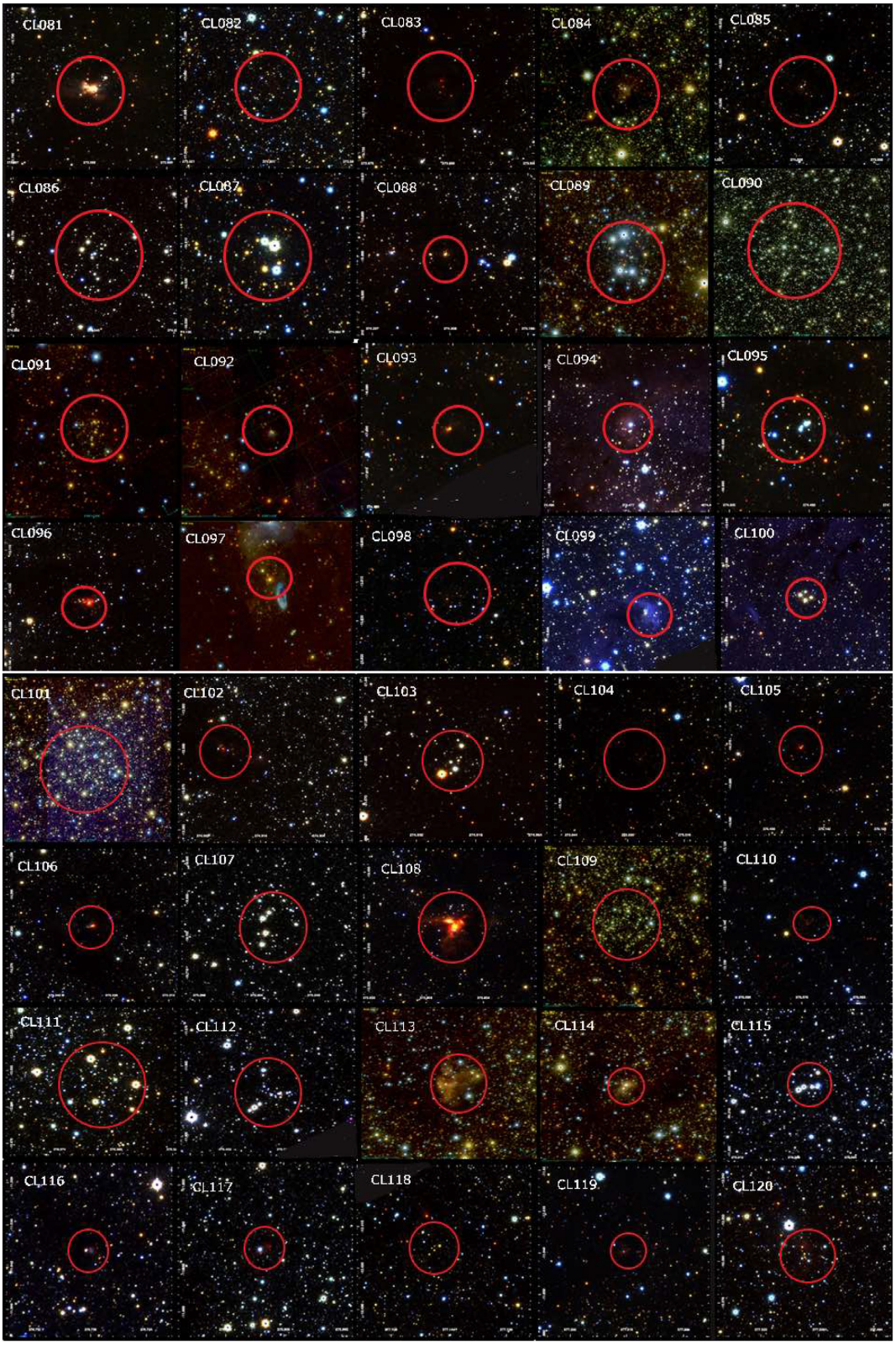

Figure C1 *continued*

APPENDIX D: COLOUR–MAGNITUDE DIAGRAMS OF SOME OF THE VVVX OPEN CLUSTER CANDIDATES.

The colour–magnitude diagrams of some of the new open cluster candidates are plotted in Fig. D1.

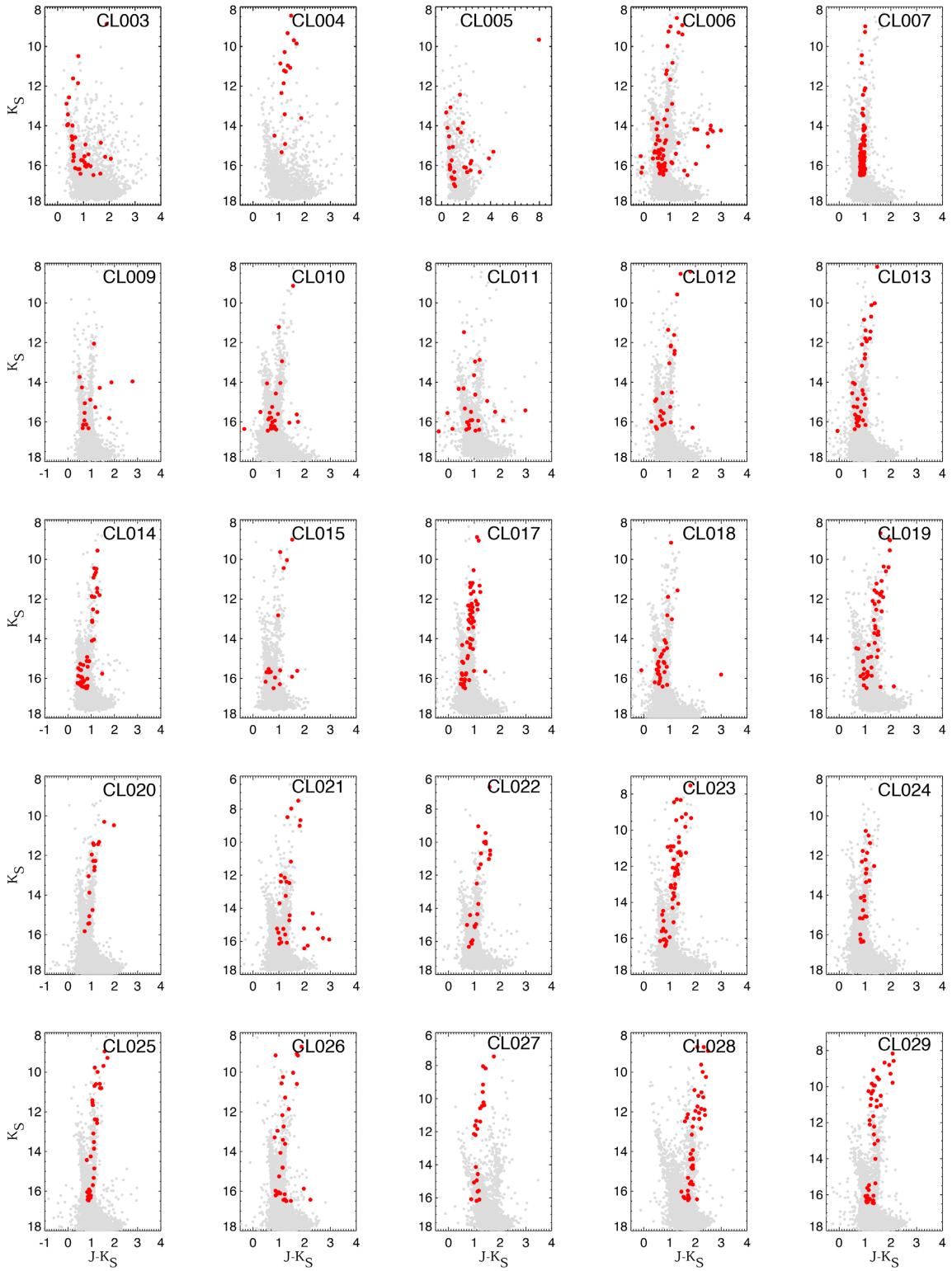

Figure D1. VVVX K_S versus $(J - K_S)$ colour–magnitude diagrams of the new open cluster candidates. The stars within 2.5 armin radius are plotted with grey points, the large red circles stand for probable cluster members.

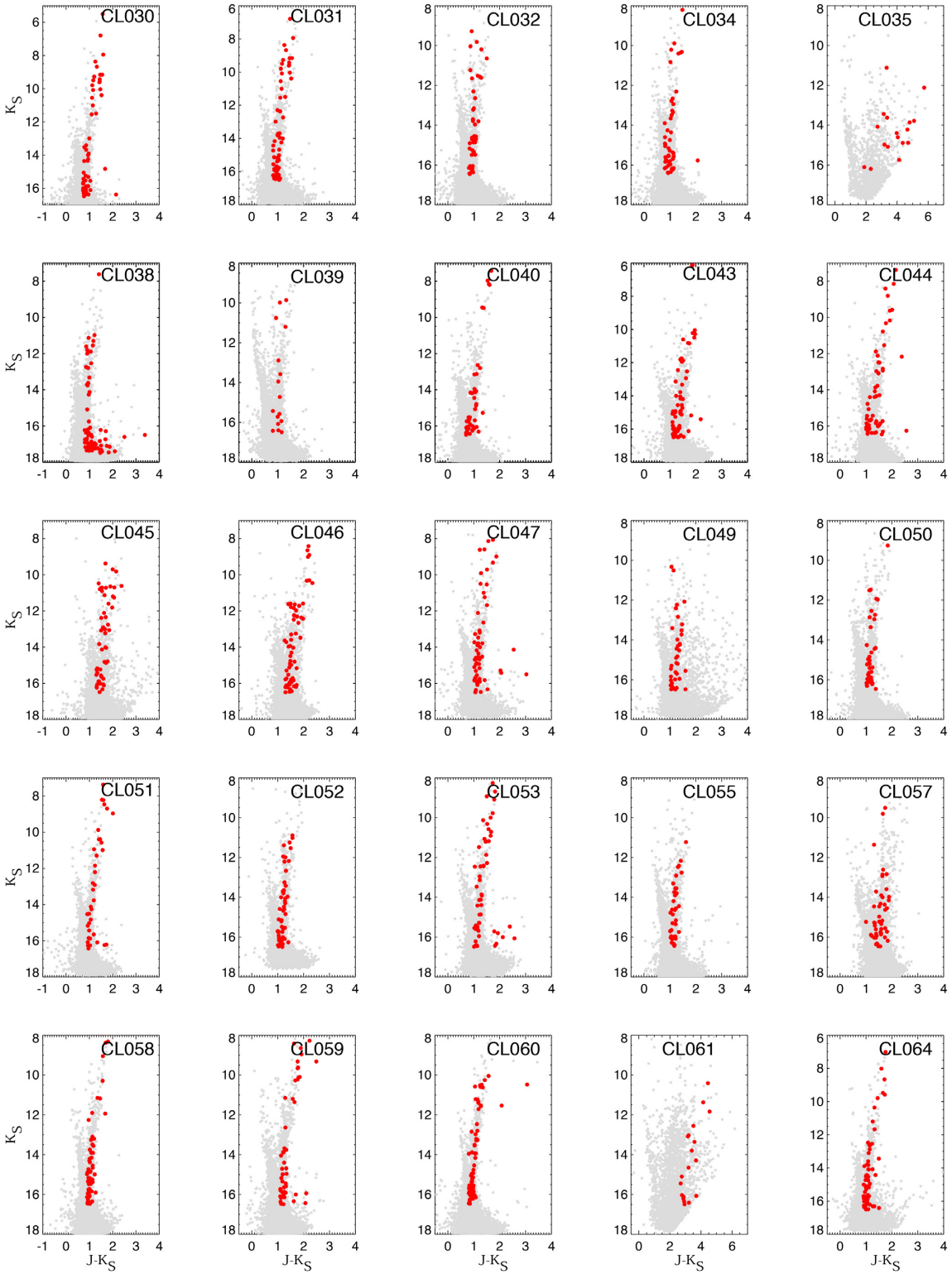

Figure D1 *continued*

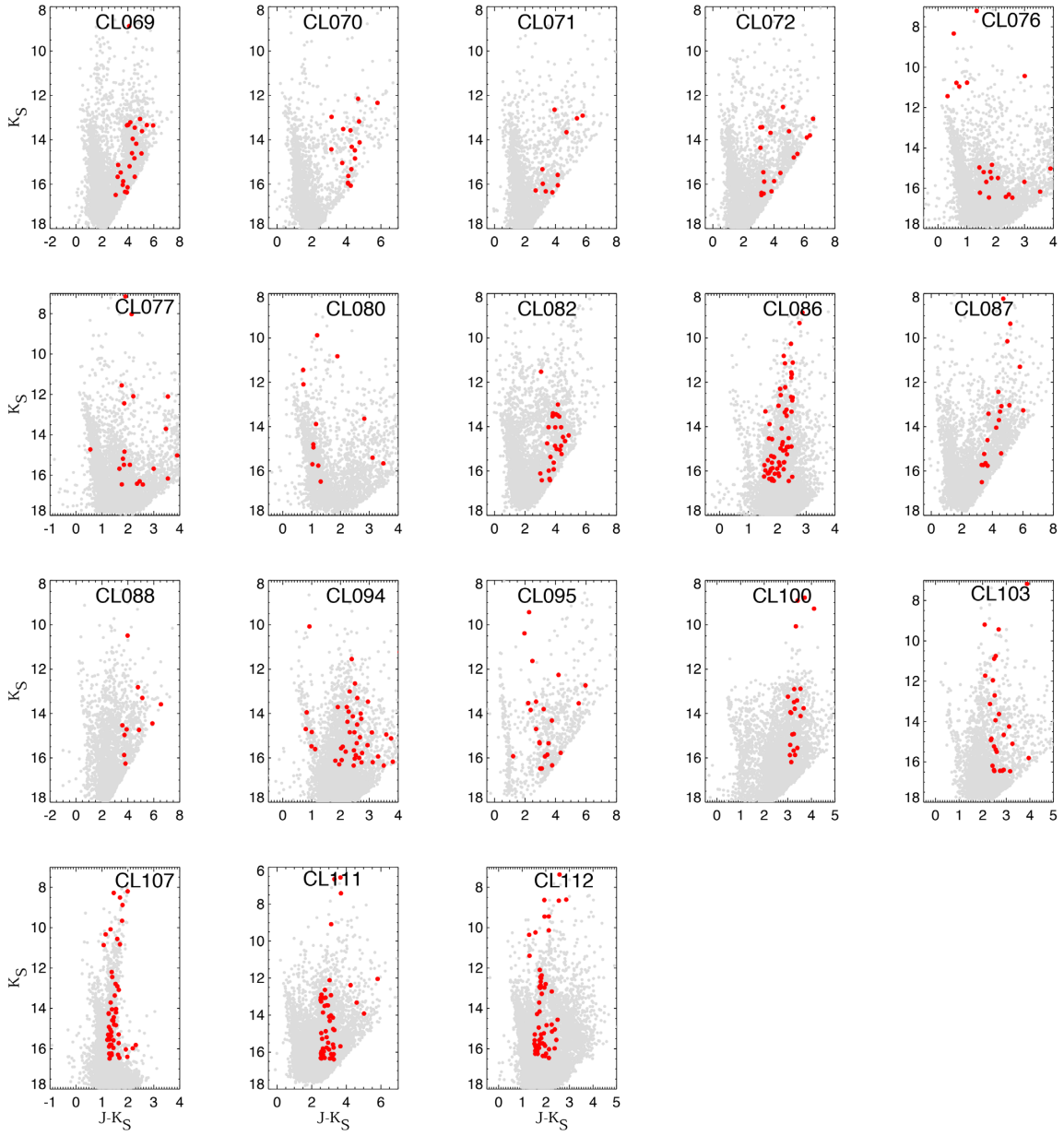

Figure D1 *continued*

This paper has been typeset from a TEX/LATEX file prepared by the author.